Slip system level strengthening in nano-indentation of single crystalline copper: numerical study via a non-local CPFEM model

Shuai Zhu[1], *Emmanuel* Brousseau[1*]

[1]Cardiff School of Engineering, Cardiff University, Cardiff CF24 3AA, United Kingdom

Abstract. A three-dimensional non-local crystal plasticity finite element model (CPFEM) integrating the evolution of geometrically necessary dislocations (GNDs) and statistically stored dislocations (SSDs) was developed to simulate the nano-indentation of single crystal copper. The simulation accurately reproduced published experimental results when considering force-depth curves, indentation size effect (ISE), anisotropic plastic deformation and sink-in phenomenon. The accumulated slip, i.e., shear strain in individual slip systems, was quantitively investigated. It is anticipated that the developed non-local CPFEM model can support future sub-micro and nanoscale manufacturing research as it enables the rapid exploration of slip system level mechanical response of a diverse range of crystalline alloys.

1 Introduction

The detailed understanding of the anisotropic behaviour of single crystals during material deformation can provide theoretical foundations to improve component quality and manufacturing efficiency [1]. Indentation testing is a widely adopted non-destructive method for characterising local material properties [2] including hardness, elastic modulus, fracture toughness, and maximum elastic recovery rate [3]. When such tests are conducted on the nano/submicron scale, the indentation size effect (ISE) is a key phenomenon resulting in the material hardness increasing as the indentation depth decreases.

It has been proposed that variations in properties for a given specimen material are attributable to strain gradients, arising from inherent inhomogeneity in the material substructure. The resulting incompatibility in slip-dominated plastic deformation processes can often be resolved by geometrically necessary dislocations (GND), atomic scale, linear crystalline defects that extend several nm to hundreds of nm in length [4]. In face-centered cubic (FCC) crystals such as copper, dislocation cores of all characters are planar, usually extended, and are relatively prone to move. Thus, the yield strength of copper is related to the stress needed for dislocations to glide and consequently activated slip systems [5]. The evolution of dislocation structures plays a crucial role in the strengthening and failure mechanisms of materials [6]. The mechanisms of dislocation motion are too fine or fast to be

* Corresponding author: BrousseauE@cardiff.ac.uk

accurately resolved experimentally and so to rationalise glide behaviour, theory and computation have been used by researchers [7].

To reveal dislocation mechanisms on fine length and time scales, various computational techniques have been employed to simulate the strengthening effect caused by dislocations. Crystal plasticity finite element method (CPFEM) is a mesoscale technique widely recognised for its ability to link dislocation-level activities with macroscale properties [8]. Wang et al., studied the crystallographic influence and indentation surface morphology of single and bi-crystalline copper [9]. Non-local CPFEM models which included GND hardening were further developed for the investigation of ISE of copper [10], zirconium alloy [11, 12], Al-8Ce-10Mg alloy [13] and austenitic stainless steels [14]. However, the quantitative contribution of strengthening from individual slip systems resulting from the accumulation of different types of dislocations induced by nanoindentation has not been fully exploited due to the complex anisotropic response during indentation. While many early seminal studies of nanoindentation of copper focused on ISE, relatively little effort has been dedicated into using numerical tools to quantify the contribution of deformation slips that may lead to a more fundamental understanding of the material plastic response.

To address the aforementioned gap, a 3D non-local CPFEM model with explicit introduction of dislocations was developed in this work. The model was employed to study the role of dislocations in the ISE, surface morphology and the anisotropic deformation behaviour of single crystal copper during nanoindentation. Simulations were designed to reveal the slip system level contribution to the strengthening effect as a function of indentation depth from 100 nm to 500 nm.

2 Methods

In this section, the non-local CPFEM framework used is briefly summarised. Next, the numerical implementation of the indentation model is described. More detailed introduction of the CPFEM framework can be found in [13] and [15].

2.1 Numerical framework

The flow rule of slip system a is expressed as [16]:

$$\dot{\gamma}^a=\dot{\gamma}_0\left(\frac{|\tau^a|}{\tau_c^a}\right)^n sgn(\tau^a) \quad (1)$$

where $\dot{\gamma}_0$ is the reference shear rate, n is the power law exponent, τ^a is the resolved shear stress on slip system a, τ_c^a is the critical resolved shear stress (crss) which describes resistance to the gliding dislocations and can be further formulated as:

$$\tau_c^a=\tau_c^0+\Delta\tau_c^a \quad (2)$$

where τ_c^0 is the initial crss and $\Delta\tau_c^a$ is the hardening caused by dislocation activities, which can be expressed as:

$$\Delta\tau_c^a=Gb^a\sqrt{\zeta^2\rho_{for}^a} \quad (3)$$

where G is the shear modulus, b is the magnitude of Burgers vector, ζ is the geometric factor, $\zeta^2\rho_{for}^a$ describes the cut-through strength obtained by forest dislocations ρ_{for}^a which can be obtained by the projection of total dislocations ρ_{tot}^a with line direction $\mathbf{t}^b$ onto a slip system with slip plane normal $\mathbf{n}^a$:

$$\rho_{for}^a=\left|\mathbf{n}^a\cdot\mathbf{t}^b\right|\rho_{tot}^b \quad (4)$$

ρ_{tot}^a can be expressed as the sum of SSD and GND densities:

$$\rho_{tot}^a=\rho_{SSD}^a+\rho_{GND}^a \quad (5)$$

The evolution of SSD density for slip system a follows the KME model [17]:

$$\Delta\rho_{SSD}^{a}=\left(k_1\sqrt{\rho_{for}^{a}}-k_2(\dot{\varepsilon},T)\rho_{SSD}^{a}\right)|\dot{\gamma}^{a}|\Delta t \quad (6)$$

The k_2 is the annihilation constant. The GND density is calculated from Nye's dislocation density tensor Λ [18], which can be expressed based on the curl of plastic deformation gradient $\boldsymbol{F}^{p}$ [19]:

$$\Lambda=(\nabla\times\boldsymbol{F}^{p^T})^T \quad (7)$$

Thus, the GND density ρ_{GND} can be obtained as:

$$\rho_{GND}=[\boldsymbol{A}]^T([\boldsymbol{A}][\boldsymbol{A}]^T)^{-1}\{\Lambda\} \quad (8)$$

where [**A**] is the linear operator matrix calculated based on slip line direction **t**, slip plane normal **n** and Burgers vector **b**. $\{\Lambda\}$ is the vector form of the Nye's dislocation density tensor Λ.

2.2 CPFEM model of nanoindentation

The developed three-dimensional CPFEM model of nanoindentation included a cylindrical single crystal copper sample and a standard Berkovich indenter. The copper sample had a height of 8 μm and a diameter of 10 μm. The copper sample was meshed with 10953 10-node quadratic tetrahedron elements of type C3D10. The bottom surface of the cylinder was fixed, and all the other surfaces were free of constraints. The contact between the Berkovich indenter and indented sample was set to be of the type "surface-to-surface contact" (Standard) with normal behaviour of 'hard' contact. Moreover, friction between the indenter and sample surface was ignored as assumed to have little effect on the force-depth relationship [20, 21]. To compare the simulation results with experimental data [10], the displacement was applied along the Z direction of the indenter (with all other degrees of freedom constrained) and increased linearly to 460 nm in 50 s before being withdrawn to the initial position in 20 s. The Euler angles, i.e., the crystallographic orientation of the single-crystal sample was 17.33°, 48.36°, 38.84°, respectively. All the equations presented in section 2.1 were compiled through a user subroutine UMAT and the model was established in the finite element software ABAQUS/Standard. The material properties used are given in Table 1 [10].

Table 1. Parameters of the CPFEM model for copper.

Parameter	Notation	Value	Notation	Notation	Value
Elastic properties	C11	168.4 GPa	Hardening constant	k_1	0.13 μm^{-1}
	C12	121.4 GPa	Dislocation interaction parameter	c	10
	C44	75.4 GPa	Effective activation enthalpy	g^a	10^{-3}
Power law exponent	n	8.8	Drag stress	D^a	300 MPa
Reference slip rate	$\dot{\gamma}_0$	10^{-3} s^{-1}	Reference slip rate	$\dot{\varepsilon}_0$	10^{7} s^{-1}
Burgers vector	b	0.255 nm	Geometric factor	ζ	0.1
Initial crss	τ_c^0	32 MPa			

3 Results and discussion

3.1 Indentation size effect

The non-local CPFEM model was applied to simulate the nano-indentation behaviour of single crystal copper. The influence of GND was examined by simulating nanoindentations without including the GND hardening. As depicted in Fig. 1(a), the simulated force-depth curve is presented as red lines (with GND), blue lines (without GND), while the experimental data [10] is shown as black lines. The results reveal a significant increase in the reaction force when GNDs are considered under the same indentation depth. The figure also illustrates that the CPFEM simulations with the GND hardening can accurately predict force-depth curves. This figure provides evidence in the ability of the developed non-local CPFEM framework to predict the mechanical behaviour of single crystal copper at the nanoscale with the consideration of GNDs.

Fig. 1(b) compares the experimentally obtained [10] and simulated changes in indentation hardness for single crystal copper. It is evident that when GNDs are considered, the nanoindentation hardness exhibits a significant ISE as observed experimentally. However, the nanoindentation hardness without considering GNDs does not result in the ISE. It should be clarified that a phenomenon somewhat similar to the ISE can also be observed in Fig. 1(b) (without GND) due to the strain-rate sensitivity of the indentation hardness [12].

Fig. 1(c) shows the evolution of the calculated GND density (averaged in the plastically deformed zone) with the indentation depth h. With the increase of indentation depth, the GND density decreases and tends to stabilise asymptotically at h ≈ 400 nm. Similar trends were evidenced in [12, 22] where the same Berkovich indenter and FCC crystal were adopted. It was reported that when 100 nm < h < 400 nm, significant ISE in FCC crystal was observed while beyond a depth of 400 nm, the hardness tended to stabilise.

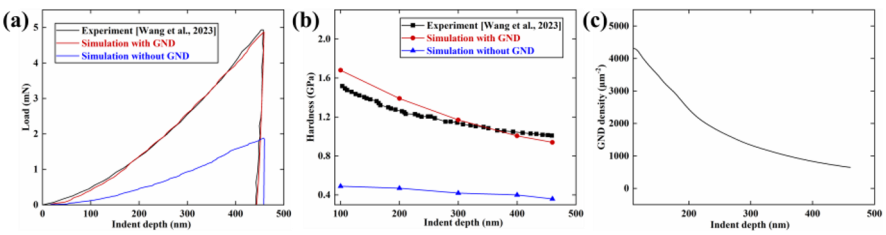

Fig. 1. Illustration of the effect of GND hardening on nanoindentation of single crystal copper (a) force-depth curve, (b) hardness-depth curve. (c) GND density-indentation depth curve.

3.2 Surface morphology

Numerical distributions for the out-of-plane displacement (U3) are presented in Fig. 2 when the indentation depth is h = 460 nm. An obvious sinking-in behaviour (marked with circles in Fig. 2. (a)) is observed for copper sample when GNDs are considered. Published research indicates that the indented region tends to sink-in for materials with high strain-hardening behaviour (e.g. copper) [23, 24]. On the contrary, indentation pile-ups are usually observed in materials with low strain-hardening potential [25], as shown in Fig. 2(b) when GNDs are not modelled. The sink-in phenomenon was also reported in the nanoindentation of other FCC crystals with an indentation depth of 550 nm [12]. Without the introduction of GNDs, as shown in Fig. 2(b), the sink-in behaviour of copper is inhibited due to the weak strain-hardening capability. Fig. 3(c) shows U3 along path a and path b as illustrated in Fig. 3(a). It is clear that sink-in and pile-up phenomena were observed in the simulations with/without

GNDs, respectively. Moreover, the anisotropic deformation along the edges were also identified.

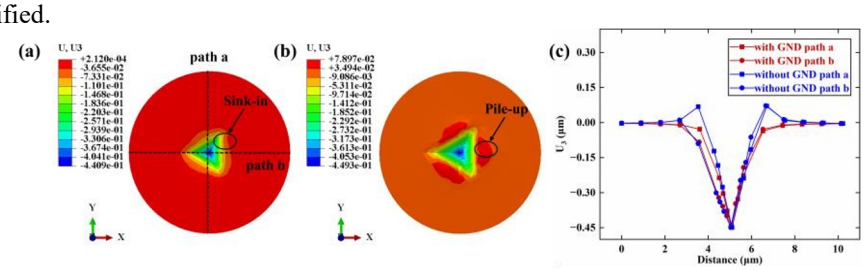

Fig. 2. Contour plots of out-of-plane displacement U3 (a) with GNDs; (b) without GNDs; (c) U3 along path a and path b.

Fig. 3 compares the distribution of equivalent plastic strain (PEEQ) in simulated samples with/without the introduction of GNDs. The indentation depth is h = 460 nm. When viewed from the indentation direction (Z direction), a triangular-shaped PEEQ region is observed in both cases (see Fig. 3(a) and (b)) due to the indenter shape. The PEEQ area without GNDs is much larger than that with GNDs, resulting in smaller nanoindentation hardness since the slip systems are more prone to be activated. The inhibited expansion of PEEQ in the GND sample mainly comes from the impediment of sliding dislocations, which enhanced its ability to deform plastically, i.e., hardened the material. The distribution of PEEQ also displays anisotropic characteristics. This slight anisotropy in the indentation behaviour can also be found in other FCC crystals [12, 13, 24].

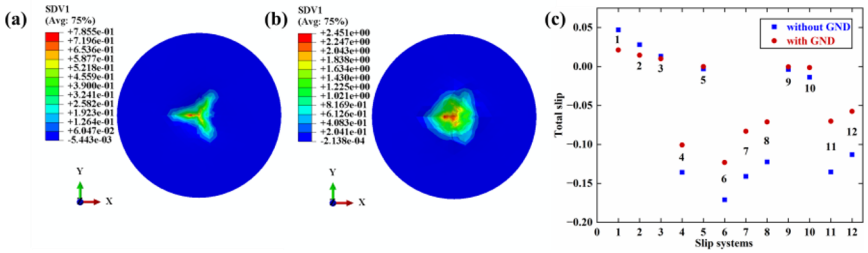

Fig. 3. The simulated distribution of equivalent plastic strain (PEEQ) with/without GND hardening. (a) with GND hardening, top view; (b) without GND hardening, top view; (c) the simulation results of total slip (shear strain) on individual slip systems.

3.3 Accumulated slip in individual slip systems

Since indentation force-depth curve, hardness and surface morphology were predicted satisfactorily via the developed non-local CPFEM model, one can have confidence in the predicted contribution of each slip system to deformation, which is otherwise difficult to access experimentally [26]. Fig. 3(c) illustrates the accumulated slip distribution i.e., shear strain within the 12-slip systems of FCC crystal. The simulated accumulated slip is found to be distinct in different slip planes and directions, as is expected during copper nanoindentation. The accumulation of slip in all 12 systems is considerably limited in the GND model comparing with non-GND model, which is aligned with the PEEQ data discussed earlier. Specifically, the accumulated slip for the non-GND model is significantly more extensive than that for the GND model especially in slip planes $(\bar{1}11)$, $(1\bar{1}1)$, and $(11\bar{1})$. This can be explained since GNDs are induced by indentation due to the presence of strain gradients which increases inversely with decreasing dimensions/depth of the indent, resulting in higher slip system resistance and material hardness [13].

Conclusions

A non-local CPFEM framework was established to study the effects of dislocations on the nanoindentation behaviour of single crystal copper. The predicted load-depth curve and indentation hardness data were found to be in good agreement with published experimental results, indicating the validity of the model. The developed CPFEM model demonstrated excellent capability to capture the nanoscale deformation behaviour of single crystal copper and forms a good basis for studying further microstructure-property relations in the context of sub-micro and nanoscale manufacturing research endeavours.

Shuai Zhu would like to thank the support of China Scholarship Council for sponsoring his PhD study at Cardiff University. Shuai Zhu would like to thank Dr Eralp Demir and Dr Zhanfeng Wang for their inspiration.

References

1. Y. Piao, C. Li, Y. Hu, H. Cui, X. Luo, Y. Geng, F. Zhang, J MATER RES TECHNOL, **28,** 4615 (2024)
2. C. A. Schuh, Mater. Today, **9,** 32 (2006)
3. C. Li, Q. Zhang, Y. Zhang, F. Zhang, X. Wang, G. Dong, Ceram. Int **46,** 3382 (2020)
4. J.P. Hirth, L. Kubin, Dislocations in Solids (Elsevier, 2009)
5. S. Wang, Z. Hu, Z. Huang, B. Gao, X. Chen, J. Hu, Y. Zhu, Y. Li, H. Zhou, Int. J. Plast **174,** 103908 (2024)
6. S.R. Kalidindi, C.A. Bronkhorst, L. Anand, J. Mech. Phys. Solids 40, 537 (1992)
7. M.R. Jones, L.T.W. Fey, I.J. Beyerlein, Comput. Mater. Sci 232, 112652 (2024)
8. F. Roters, P. Eisenlohr, L. Hantcherli, D.D. Tjahjanto, T.R. Bieler, D. Raabe, Acta Mater, **58,** 1152 (2010)
9. Z. Wang, J. Zhang, H.U. Hassan, J. Zhang, Y. Yan, A. Hartmaier, T. Sun, Int. J. Mech. Sci **148,** 531(2018)
10. Z. Wang, X. Liu, S.Wu, W. Liu, R. Yang, B. Jiang, Mater. Charact **203,** 113142 (2023)
11. X.D. Zan, X. Guo, G.J. Weng, Int. J. Plast **174,** 103911 (2024)
12. X.D. Zan, X. Guo, G.J. Weng, G. Chen, Int. J. Plast **167,** 103675 (2023)
13. J. Cheng, R. Lane, M.S. Kesler, J. Brechtl, X. Hu, R. Mirzaeifar, O. Rios, A. M. Momen, K. Nawaz, Int. J. Solids Struct **233,** 111233 (2021).
14. D. Agius, A. Kareer, A.A. Mamun, C. Truman, D.M. Collins, M. Mostafavi, D. Knowles, Int. J. Plast **152,** 103249. (2022)
15. V. Kuksenko, S. Roberts, E. Tarleton, Int. J. Plast **116,** 62 (2019)
16. M. F.Ashby, Philos. Mag **21,** 399 (1970)
17. H. Mecking, U.F. Kocks, Acta Metall. Sinica **29,** 1865 (1981)
18. J.F. Nye, Acta Metall. Sinica **1,** 153 (1953)
19. A. Arsenlis, D.M. Parks, Acta Mater **47,** 1597 (1999)
20. Y. Wang, D. Raabe, C. Klüber, F. Roters, Acta Mater **52,** 2229 (2004)
21. M. Liu, A.K. Tieu, C. Lu, H. Zhu, G. Deng, Comput. Mater. Sci **81,** 30 (2014)
22. M.N. Cinbiz, M. Balooch, X. Hu, A Amroussia, K. Terrani, J. Alloys Compd **726,** 41 (2017)
23. S. Kucharski, D. Jarząbek, METALL MATER TRANS A 45, 4997 (2014)
24. X. Xiao, L. Chen, L. Yu, H. Duan, Int. J. Plast **116,** 216 (2019)
25. S, Huang, C. Zhou, JOM **69,** 2256 (2017)
26. R.J. McCabe, L. Capolungo, P.E. Marshall, C.M. Cady, C.N. Tomé, Acta Mater **58,** 5447 (2010)